Redox Biology 73 (2024) 103179

Contents lists available at ScienceDirect

Redox Biology

journal homepage: www.elsevier.com/locate/redox

Mitochondrial GPX4 acetylation is involved in cadmium-induced renal cell ferroptosis

Yue-Yue Guo [a,1], Nan-Nan Liang [a,1], Xiao-Yi Zhang [a,1], Ya-Hui Ren [b], Wen-Zheng Wu [b], Zhi-Bing Liu [c], Yi-Zhang He [b], Yi-Hao Zhang [a], Yi-Chao Huang [a], Tao Zhang [b], De-Xiang Xu [a,**], Shen Xu [b,*]

[a] Department of Toxicology, Anhui Medical University, Hefei, 230032, China
[b] Department of Urology, The Second Affiliated Hospital of Anhui Medical University, Hefei, 230601, China
[c] Department of Blood Transfusion, The Second Affiliated Hospital of Anhui Medical University, Hefei, Anhui, China

ARTICLE INFO

Keywords:
Acute kidney injury
Ferroptosis
Mitochondrial lipid peroxidation
Mitochondrial GPX4 acetylation
SIRT3
Nicotinamide mononucleotide

ABSTRACT

Increasing evidences demonstrate that environmental stressors are important inducers of acute kidney injury (AKI). This study aimed to investigate the impact of exposure to Cd, an environmental stressor, on renal cell ferroptosis. Transcriptomics analyses showed that arachidonic acid (ARA) metabolic pathway was disrupted in Cd-exposed mouse kidneys. Targeted metabolomics showed that renal oxidized ARA metabolites were increased in Cd-exposed mice. Renal 4-HNE, MDA, and ACSL4, were upregulated in Cd-exposed mouse kidneys. Consistent with animal experiments, the in vitro experiments showed that mitochondrial oxidized lipids were elevated in Cd-exposed HK-2 cells. Ultrastructure showed mitochondrial membrane rupture in Cd-exposed mouse kidneys. Mitochondrial cristae were accordingly reduced in Cd-exposed mouse kidneys. Mitochondrial SIRT3, an NAD^+-dependent deacetylase that regulates mitochondrial protein stability, was reduced in Cd-exposed mouse kidneys. Subsequently, mitochondrial GPX4 acetylation was elevated and mitochondrial GPX4 protein was reduced in Cd-exposed mouse kidneys. Interestingly, Cd-induced mitochondrial GPX4 acetylation and renal cell ferroptosis were exacerbated in $Sirt3^{-/-}$ mice. Conversely, Cd-induced mitochondrial oxidized lipids were attenuated in nicotinamide mononucleotide (NMN)-pretreated HK-2 cells. Moreover, Cd-evoked mitochondrial GPX4 acetylation and renal cell ferroptosis were alleviated in NMN-pretreated mouse kidneys. These results suggest that mitochondrial GPX4 acetylation, probably caused by SIRT3 downregulation, is involved in Cd-evoked renal cell ferroptosis.

1. Introduction

Acute kidney injury (AKI) refers to acute renal dysfunction accompanied by severe tubular damage [1,2]. It is generally believed that sepsis caused by bacterial infection, acute renal ischemia caused by various reasons, and acute poisoning caused by drugs, are the main causes of clinical AKI [3,4]. Recently, Numerous researches have demonstrated that environmental stressors are the important inducers of AKI [5,6]. Cadmium (Cd) is a well-known environmental stressor, widely distributed in polluted water, atmosphere, soil, and food [7–10]. Cd is highly toxic and non-biodegradable and has a half-life of 10–30 years [11]. Numerous studies have indicated that environmental Cd exposure causes damage of multiple organs, including testicles, liver, kidney, bones and lungs [12–16]. Indeed, kidney is a major accumulation organ of Cd, and former studies have shown that chronic exposure to cadmium can trigger renal dysfunction [17,18]. It has been shown in several animal studies that exposed Cd acutely results AKI [19,20].

It is widely recognized that necrosis and apoptosis are the major modes of renal cell death involved in AKI pathogenesis [21]. On the other hand, autophagy was a protective mechanism against AKI [22]. Several studies have demonstrated that necroptosis is partially participated in AKI caused by ischemia-reperfusion induced acute kidney injury [23]. Ferroptosis, a novel regulatory cell death characterized by intracellular free iron overload and membrane lipid peroxidation [24]. Excessive reactive oxygen species (ROS)-mediated lipid peroxidation in

* Corresponding author. The Second Affiliated Hospital, Anhui Medical University, Hefei, 230601, China.
** Corresponding author.
E-mail addresses: xudex@126.com (D.-X. Xu), xushen01@126.com (S. Xu).
[1] These authors contributed equally to this work.

https://doi.org/10.1016/j.redox.2024.103179
Received 18 April 2024; Accepted 1 May 2024
Available online 8 May 2024

Abbreviations

AKI	Acute kidney injury
$CdCl_2$	Cadmium Chloride
NMN	Nicotinamide Mononucleotide
BUN	Blood Urea Nitrogen
UA	Uric Acid
Scr	Serum creatinine
MDA	Malondialdehyde
H&E	Hematoxylin-eosin
ARA	Arachidonic acid
ALA	linolenic acid
DHA	Docosahexaenoic acid
EPA	Eicosapentaenoic acid
LA	Linoleic acid

membrane structures triggers ferroptosis [24]. Recently, numerous studies demonstrate that failure of defensive mechanisms, including glutathione peroxidase 4 (GPX4) and ferroptosis suppressor protein 1 (FSP1), is an important reason for ferroptosis [25–27]. A study showed that acute Cd exposure can lead to ferroptosis in renal cells [19]. However, the potential mechanism of Cd-induced ferroptosis is not completely clear.

The aim of this study was to investigate the impact of acute Cd exposure on ferroptosis in renal cells. The in vivo and in vitro experiments found that acute Cd exposure caused mitochondrial lipid peroxidation. Our results demonstrate that mitochondrial GPX4 acetylation is involved in Cd-induced renal cell ferroptosis. We provide novel evidence that SIRT3 downregulation partially contributes to Cd-evoked mitochondrial GPX4 acetylation and renal cell ferroptosis. Nicotinamide mononucleotide (NMN), a precursor for cellular NAD^+ synthesis, could efficiently protect against environmental stressor induced renal cell ferroptosis and AKI.

2. Materials and methods

2.1. Chemicals and reagents

$CdCl_2$ (No: 202908) was from Sigma-Aldrich (MO, USA). Nicotinamide mononucleotide (NMN, No: 1094-61-7) was from Aladdin (Shanghai, China). Antibodies against ACSL4 (No: sc-365230) and SIRT3 (No: sc-365175) were from Santa Cruz (CA, USA). Antibodies against acetylated-lysine (No: 9441) and TOM20 (No: 42406) were from Cell Signaling Technology (Danvers, MA, USA). Antibody against FSP1 (No: 20886-1-AP) was from Proteintech (Wuhan, China). Antibodies against 4-hydroxynonenal (4-HNE, No: ab46545), SIRT3 (No: ab246522) and GPX4 (No: ab125066) were from Abcam (Cambridge, MA, USA). Antibody against VDAC1 (No: SAB5700655) was from Sigma (MO, USA). The secondary antibodies conjugated with fluorochrome, such as Alexa Fluor 350-labeled goat anti-rabbit IgG (No: A0408), Alexa Fluor 488-labeled goat anti-rabbit IgG (No: A0423) and Cy3-labeled goat anti-mouse IgG (No: A0521) were from Beyotime (Shanghai, China). Cell Counting Kit-8 (CCK-8, No: BS350A) was from Biosharp (Hefei, China). HRP-linked polymer detection system was from Golden Bridge International (WA, USA). Kidney function detection kits were obtained from ERKN Biological Technology (Wenzhou, China). Malondialdehyde (MDA, No: A003–1-2) assay kit was from Nanjing Jiancheng Bioengineering Institute (Nanjing, China). JC-1 assay kits (No: C2003S) and Mito-Tracker Green (No: C1048) were from Beyotime (Shanghai, China). BODIPY™ 581/591 C11 (No: D3861) was from Thermo Fisher Scientific (Shanghai, China).

2.2. Animal experiment

Adult BALB/c male mouse (Beijing Vital River, 7-week-old, 19–21 g) were used to construct a model of Cd-induced ferroptosis and to verify the protection of NMN against Cd-induced ferroptosis in kidney. Adult male wild type C57BL/6JGpt mouse and C57BL/6JGpt Sirt3$^{-/-}$ mouse (GemPharmatech, 7-week-old, 19–23 g) were used for validation of the role of SIRT3 in Cd-induced ferroptosis in the kidney. All mice were acclimatized for 1 week with freely available food and water at temperature (20–25 °C) and humidity (50 ± 5 %). This study included four independent experiments. In the first experiment, adult male BALB/c mice were intraperitoneally injected with $CdCl_2$ (0, 2 or 4 mg/kg). Kidney tissues and blood sera were collected 24 h after $CdCl_2$. In the second experiment, adult male BALB/c mice were injected intraperitoneally with $CdCl_2$ (4 mg/kg) for 0, 6, 12 or 24 h. Kidney tissues and blood sera were collected. In the third experiment, wild type and C57BL/6JGpt Sirt3$^{-/-}$ mice were injected intraperitoneally with $CdCl_2$ (4 mg/kg). Kidney tissues and blood were collected 24 h after $CdCl_2$ injection. In the fourth experiment, adult BALB/c male mice were injected intraperitoneally with $CdCl_2$ (4 mg/kg). Mouse was pretreated with NMN (500 mg/kg) daily for five consecutive days before $CdCl_2$ injection in the NMN + Cd group. In the study, the dose of NMN referred to other study [28]. Kidney and blood were collected 24 h after $CdCl_2$ injection. All experimental protocols followed the humanitarian treatment guidelines established by the Association for Laboratory Animal Science and the Center for Laboratory Animal Science at Anhui Medical University (approval number: LLSC20220654).

2.3. Cell culture

Human proximal tubular epithelial cells (HK-2 cells) were grown in DMEM: F-12 (1:1) medium supplemented with FBS (5 %) and penicillin-streptomycin (100 units/mL). The vitro study consisted of three independent experiments. Experiment 1, to determine the dose of $CdCl_2$ induced cell death, HK-2 cells were co-culture with 0,1, 5, 10, 20 or 40 μM $CdCl_2$ for 24 h. Experiment 2, HK-2 cells were incubated with $CdCl_2$ (10 μM) for 0, 6, and 24 h to verify that $CdCl_2$ induces ferroptosis in renal cells. Experiment 3, to verify that $CdCl_2$ induces SIRT3 downregulation and mediates ferroptosis, HK-2 cells were pretreated with NMN (1 mM) for 2 h, and then $CdCl_2$ (10 μM) treatment for 24 h. The dose of NMN referred to the previous study [29].

2.4. Biochemical measurement

The blood samples were taken 24 h after Cd exposure and rested on ice followed by centrifugation at 3500 rpm × 15mins at 4 °C. Serum creatinine (Scr), Blood Urea Nitrogen (BUN) and Uric acid (UA) was detected by biochemical detector.

2.5. RNA sequencing

Total RNAs were extracted from mouse kidneys and examined for purity, content and integrity by Agilent 2100 Bioanalyzer. In this study, mRNA with polyA structure in total RNAs was enriched by Oligo(dT) magnetic beads, and mRNA was decomposed into fragments of about 300 bp in length, and then cDNA was synthesized using random primers and reverse transcriptase. The cDNA was amplified and enriched by PCR and then screened according to the size of the fragments (450 bp). After constructing the library, the enriched fragments were amplified. Finally, the libraries were subjected to paired-end (PE) sequencing by Next-Generation Sequencing (NGS). Volcano map was produced by bioinformatics. GO and KEGG pathway enrichment analyses were conducted using bioinformatics.

2.6. Histopathology and immunohistochemistry

Kidney tissue was taken and immediately fixed in 4 % paraformaldehyde, dehydrated through a series of alcohols, immersed in paraffin, solidified, and sectioned. Sections were stained with hematoxylin and eosin to visualize renal structures. The degree of renal tubular injury was analyzed according to the previous method (Paller et al. [30]). Briefly, under × 400 magnification, 10 fields were taken randomly from 100 renal tubules. The results were shown as follow: evident renal tubule expansion and flat cells (1); the appearance of tube-type cells in renal tubules (2); the appearance of some exfoliated necrotic cells in the lumen of the renal tubules but not tubular or cell fragments (1); vacuolar degeneration (1); and karyopyknosis (1). For immunohistochemistry (IHC), sections were deparaffinized, hydrated, quenched for endogenous peroxidase and antigen repair, and incubated with 4-HNE antibody (1:200) overnight at 4 °C, and at 37 °C for another 0.5 h. The corresponding secondary antibody and HRP-linked polymers were attached and nuclei were stained with hematoxylin. For renal immunofluorescence (IF), fluorescent secondary antibody was used instead of HRP-conjugated polymers and nuclei were stained with Hoechst. Sections were observed using confocal microscope (Leica THUNDER DMi8).

2.7. MDA measurement

Briefly, about 50 mg fresh kidney and 900 μl pre-cooled stroke-physiological saline solution were used to prepare tissue homogenate. The homogenate was centrifuged at 800g at 4 °C for 15 min. 200 μL supernatant was collected after centrifugation. Add the test reagent in accordance with proportion of the instructions, then put in thermostat water bath at 95 °C for 45 min. Subsequently, centrifuge at 800 g at 4 °C for 10 min. Finally, supernatant was used to detect the absorbance by microplate reader (BioTek).

2.8. Cell viability assay

HK-2 cells were seeded in 96-well plates at appropriate cell density. At the end of Cd exposure, the plates were washed with PBS and 10 μL of CCK8 solution was added to each well to determine cell viability. Cell viability was determined at 450 nm.

2.9. Detection of oxidized lipids using C11-BODIPY

For measurement of oxidized lipids, HK-2 cells were cultivated in 12-well plates. The probe for C11-BODIPY (10 μM) was added to cell medium and incubated at 37 °C for 30 min. The reduced lipids were detected at 581/591 nm and the oxidized lipids were detected at 488/510 nm after HK-2 cells were washed with PBS.

2.10. Detection of oxidized lipids using LC-MS/MS

Renal samples were thawed on ice. 200 μL of methanol/acetonitrile (1:1, v/v) solution containing internal standard was added to 20 mg renal samples. The mixture was homogenized for 20 s and the proteins were precipitated at −20 °C for 30 min. Samples were centrifuged at 12000 rpm at4 °C for 10 min. The supernatant was collected and transferred. Extract the eicosanoids from the supernatant using a PolySery MAX SPE column (ANPEL). Prior to analysis, the eluate was dried under vacuum and redissolved in 100 μL methanol/water (1:1, v/v) for UPLC/MS/MS analysis. The extracts were analyzed using an LC-ESI-MS/MS system (UPLC, ExionLC AD, https://sciex.com.cn/; MS, QTRAP® 6500+ System, https://sciex.com/).

2.11. MitoPeDPP assay

MitoPeDPP staining was used to observe oxidized lipids in mitochondria. Briefly, HK-2 cells were cultured in 12-well plates. In dark, 0.2 μmol/L MitoPeDPP working solution was co-cultured with HK-2 at 37 °C for 15 min. The results were recorded by confocal microscope (Leica THUNDER DMi8).

2.12. Mitochondrial ultrastructure

1 mm^3 fresh renal cortex was quickly fixed in 2.50 % glutaraldehyde (GA) at 4 °C. The tissue was dehydrated, embedded, and cut into ultrathin sections, then doubly stained with uranium lead.

2.13. Mitochondrial and cytoplasm protein extraction

About 50 mg fresh kidney and 1 mL pre-cooled Him buffer were used to prepare tissue homogenate. The homogenate was centrifuged at 400 g for 5 min at 4 °C. The supernatant was collected and centrifuged at 10000 g for 10 min at 4 °C. The supernatant contained cytoplasmic proteins and the precipitate was mitochondria. The precipitate was washed with Him's buffer and centrifuged at 12000 g for 10 min at 4 °C. The supernatant was discarded and an appropriate amount of buffer was added for subsequent experiments.

2.14. Co-immunoprecipitation (Co-IP)

About 500 μg mitochondrial proteins were diluted to a total volume of 600 μl. Add 10 μL A/G-agarose beads and spin at 4 °C for 2 h. Add 1 μg primary antibody and spin at 4 °C for 3 h, discard supernatant and collect agarose beads. After washing, add 30 μL 1 × lodding buffer and boil for 10 min to denature, then centrifuged at 12000 g/min for 60 s at 4 °C. The supernatant after centrifugation was used for Western blotting.

2.15. Identification of knockout mouse

Briefly, mouse tail was digested and centrifuged at 12,000 r/min. Anhydrous ethanol was added, gently shaken until a white flocculence, then centrifuged at 12,000 r/min for 15 min. The precipitate was retained and the DNA was purged with 70 % ethanol, and the procedure was repeated for two times. The DNA was dissolved in deionized water and genotyped by agarose gel electrophoresis.

2.16. Western blotting

Proteins were extracted and protein concentrations were standardized. The proteins were boiled, separated by SDS-PAGE, and transferred to a PVDF membrane. The membrane was blocked with fat-free 5 % milk. After incubation with the corresponding primary and secondary antibodies, protein expression was observed by the ChemiDoc™Touch Imaging System (BioRad).

2.17. Mitochondrial membrane potential assay (MMP)

In short, JC-1 probe is diluted 200x becoming JC-1 working solution. HK-2 cells were incubated with JC-1 working solution in the dark at 37 °C for 20 min. The results of JC-1 staining were observed and recorded by flow cytometry.

2.18. Statistical analysis

All data are presented as mean ± S.E.M. For normally distributed quantitative data, Student's t-test was applied to compare difference between two groups. One-way analysis of variance (ANOVA) and LSD post hoc tests were used to compare difference among three or more groups. For non-normally distributed data, Kruskal-Wallis test was used for comparing difference among different groups.

3. Results

3.1. Cd exposure induces changes in lipid metabolic pathway in mouse kidneys

No mouse died in the experiment. A single dose of Cd exposure did not influence body weight, kidneys weight and kidneys coefficient (Supplementary Figs. 1A–C). As shown in Fig. 1A, nuclear consolidation and brush border detachment were observed in Cd-exposed mouse kidneys. Quantitative analysis displayed that pathological score was elevated in Cd-exposed mouse kidneys (Fig. 1B). Renal function indicators were measured. Despite no difference on Scr and BUN (Fig. 1C and D), serum UA level was elevated in Cd-exposed mice (Fig. 1E). Kidney injury molecule 1(Kim-1) was then detected using Western blot. Kim-1 was elevated in Cd-exposed mouse kidneys (Fig. 1F and G). Next, renal pathology and serum UA were analyzed at different time points after Cd exposure. As shown in Fig. 1H, brush border detachment and tubular pattern were shown in the renal tubules of Cd-exposed mouse kidneys. Time-course analysis showed that pathological damage began at 12 h and aggravated at 24 h after Cd exposure (Fig. 1I). Accordingly, serum UA level was elevated in Cd-exposed mice, beginning at 12 h and further aggravating at 24 h after Cd exposure (Fig. 1J). To screen the potential mechanism for Cd-induced AKI, transcriptomics analyses were performed in mouse kidneys. As presented in Fig. 1K, genome-wide expression profile showed obvious changes in Cd-exposed mouse kidneys, with 193 DEGs down-regulated and 270 DEGs up-regulated. KEGG analyses showed that DEGs were enriched in cellular metabolic pathway, such as glucose metabolism, lipid metabolism, and amino acid metabolism (Fig. 1L). Lipid metabolic pathway was further analyzed (Fig. 1M) and found that arachidonic acid (ARA) metabolism, a critical pathway for ferroptosis, was markedly disturbed in Cd-exposed mouse kidneys (Fig. 1N).

3.2. Cd exposure induces lipid peroxidation in mouse kidneys and HK-2 cells

The major cause of ferroptosis is lipid peroxidation of ARA. Targeted metabolomics of oxidized lipids were then analyzed using LC-MS/MS. Heat map showed that an obvious difference in oxidized lipids was observed between Cd-exposed mouse kidneys and controls (Fig. 2A). Quantitative analysis displayed that oxidized arachidonic acid (ARA) metabolites, including 20-COOH-LTB4, 12-*epi*-LTB4, LXA4, 20-HETE, 19(s)HETE, 18-HETE, 17-HETE and TXB2, were increased in Cd-exposed mouse kidneys (Fig. 2B). Other oxidized lipid metabolites, such as docosahexaenoic acid (DHA), linolenic acid (ALA), eicosapentaenoic acid (EPA) and linoleic acid (LA), were elevated in Cd-exposed mouse kidneys (Fig. 2C–F). Renal 4-HNE and MDA, two indexes of ferroptosis, were analyzed. As shown in Fig. 2G–I, Renal MDA contents and 4-HNE^{+} area were upregulated in Cd-exposed mouse. Next, acyl-CoA synthetase long chain family member 4 (ACSL4), a key molecule of ferroptosis, was measured in mouse kidneys (Fig. 2J). The results showed that renal ACSL4 was up-regulated in Cd-exposed mice (Fig. 2K). The impact of Cd exposure on cell viability was analyzed in HK-2 cells. As shown in Fig. 2L, cell viability was reduced in Cd-exposed

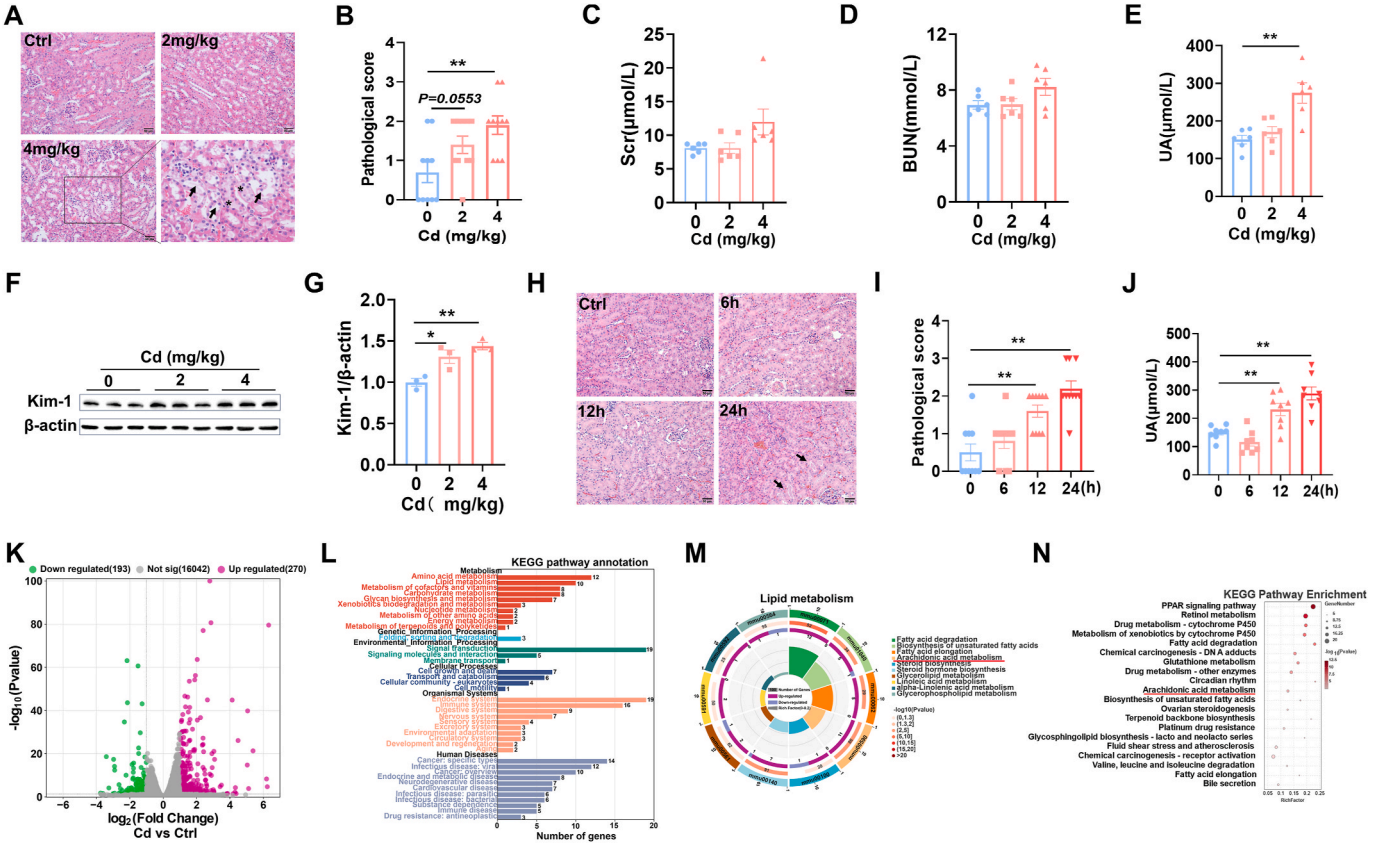

Fig. 1. Acute Cd exposure induces acute kidney injury and changes in renal lipid metabolic pathway. $CdCl_2$ (2 mg/kg or 4 mg/kg) was injected intraperitoneally into adult BALB/c male mice. Kidney tissues and blood sera were taken 24 h after $CdCl_2$. (A and B) Renal pathology was assessed. (A) Representative H&E images. (B) Pathological score. (C) Scr. (D) BUN. (E) Serum UA. (F and G) Kim-1 was measured by immunoblot. (F) Representative images. (G) Kim-1/β-actin. $CdCl_2$ was injected intraperitoneally into adult BALB/c male mice for 0, 6, 12 and 24 h (4 mg/kg), respectively. Kidney tissues and blood were taken 24 h after $CdCl_2$. (H and I) Renal pathology was assessed. (H) Representative H&E images. (I) Pathological score. (J) Serum UA. (K–N) Transcriptome analyses were performed in Cd-exposed mice kidney. (K) Scatter plot. (L) The KEGG pathway enrichment was analyzed. (M) Lipid metabolic pathways were analyzed. (N) Top of KEGG pathway was enriched. All data are presented as mean ± S.E.M. (N = 6–8). $^{*}P < 0.05$, $^{**}P < 0.01$.

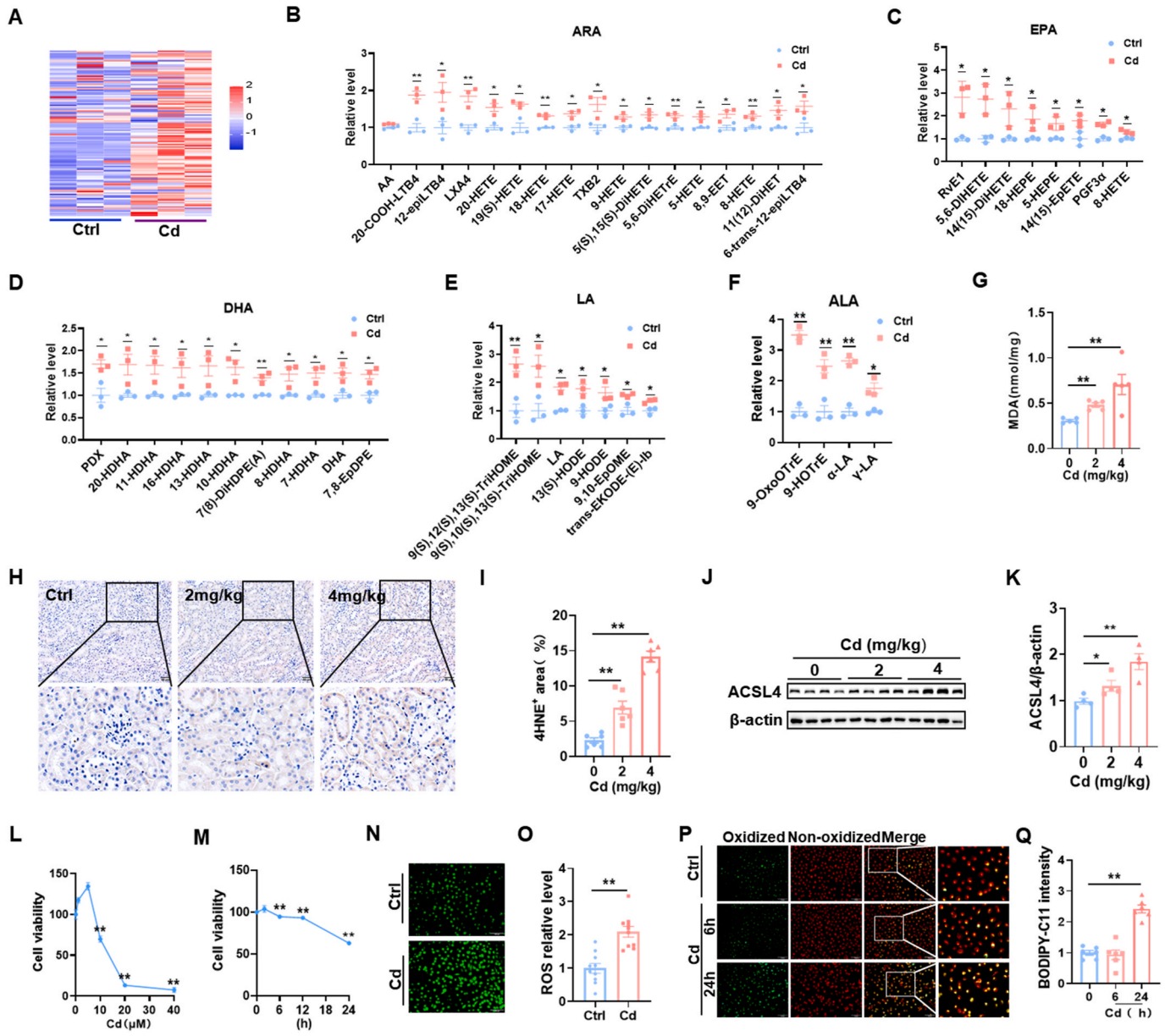

Fig. 2. Cd exposure induces lipid peroxidation in mice kidneys and HK-2 cells. (A–K) $CdCl_2$ (2 mg/kg or 4 mg/kg) was injected intraperitoneally into adult BALB/c male mice. Kidney tissues were taken 24 h after $CdCl_2$. (A–F) Targeted metabolomics of oxidized lipids were examined. (A) A heatmap. (B–G) Renal oxidized metabolites of (B) ARA, (C) EPA, (D) DHA, (E) LA and (F) ALA. (G) Renal MDA content. (H and I) Renal 4-HNE^+ area was evaluated by IHC. (H) Representative images. (I) Renal 4-HNE^+ area. (J–K) ACSL4 was detected by immunoblot. (J) Representative images. (K) ACSL4/β-actin. HK-2 cells were co-cultured different doses with $CdCl_2$ for 24 h. (L) Cell viability. HK-2 cells were co-cultured for different times with $CdCl_2$ (10 μM). (M) Cell viability. (N and O) HK-2 cells were co-cultivated with $CdCl_2$ (10 μM) for 24 h. ROS was detected by immunofluorescence. (N) Representative images. (O) Quantitative analysis. (P and Q) HK-2 cells were co-cultivated with $CdCl_2$ (10 μM) for 6 or 24 h. C11-BODIPY was used for detection of oxidized lipids. (P) Representative images. (Q) Quantitative analysis. All data are presented as mean ± S.E.M. (N = 6). $^*P < 0.05$, $^{**}P < 0.01$.

HK-2 cells in a concentration-dependent manner. Time-course analysis showed that HK-2 cell viability began to decline 6 h after Cd exposure and more than 40 % cells dead at 24 h after Cd exposure (Fig. 2M). Finally, cellular ROS and oxidized lipids were measured in HK-2 cells. As expected, ROS level was elevated in Cd-exposed HK-2 cells (Fig. 2N and O). Oxidized lipids were evaluated using C11-BODIPY (Fig. 2P). Accordingly, oxidized lipids, as determined by C11-BODIPY probe, were elevated in Cd-exposed HK-2 cells (Fig. 2Q).

3.3. Cd causes mitochondrial lipid peroxidation and structural damage in mouse kidneys and HK-2 cells

Firstly, mitochondrial lipid peroxidation was detected using MitoDePDD by confocal microscopy (Fig. 3A). As expected, a strong mitochondrial lipid peroxidation was shown in Cd-exposed HK-2 cells (Fig. 3B). Mitochondrial lipid peroxidation was further evaluated by flow cytometry (Fig. 3C). As shown in Fig. 3D, oxidized lipid content was significantly increased in Cd-exposed HK-2 cells. Next, Mitochondrial membrane potentials (MMPs) were analyzed by flow cytometry (Fig. 3E). As expected, MMPs were significantly reduced in Cd-exposed HK-2 cells (Fig. 3F). 4-HNE and TOM20 were co-localized by immunofluorescence. As expected, 4-HNE was predominantly present in mitochondria (Fig. 3G). Mitochondrial membrane rupture is the major features of cell ferroptosis [30]. The integrity of renal mitochondrial membrane was analyzed by transmission electron microscopy. As expected, rupture of mitochondrial membranes was observed in

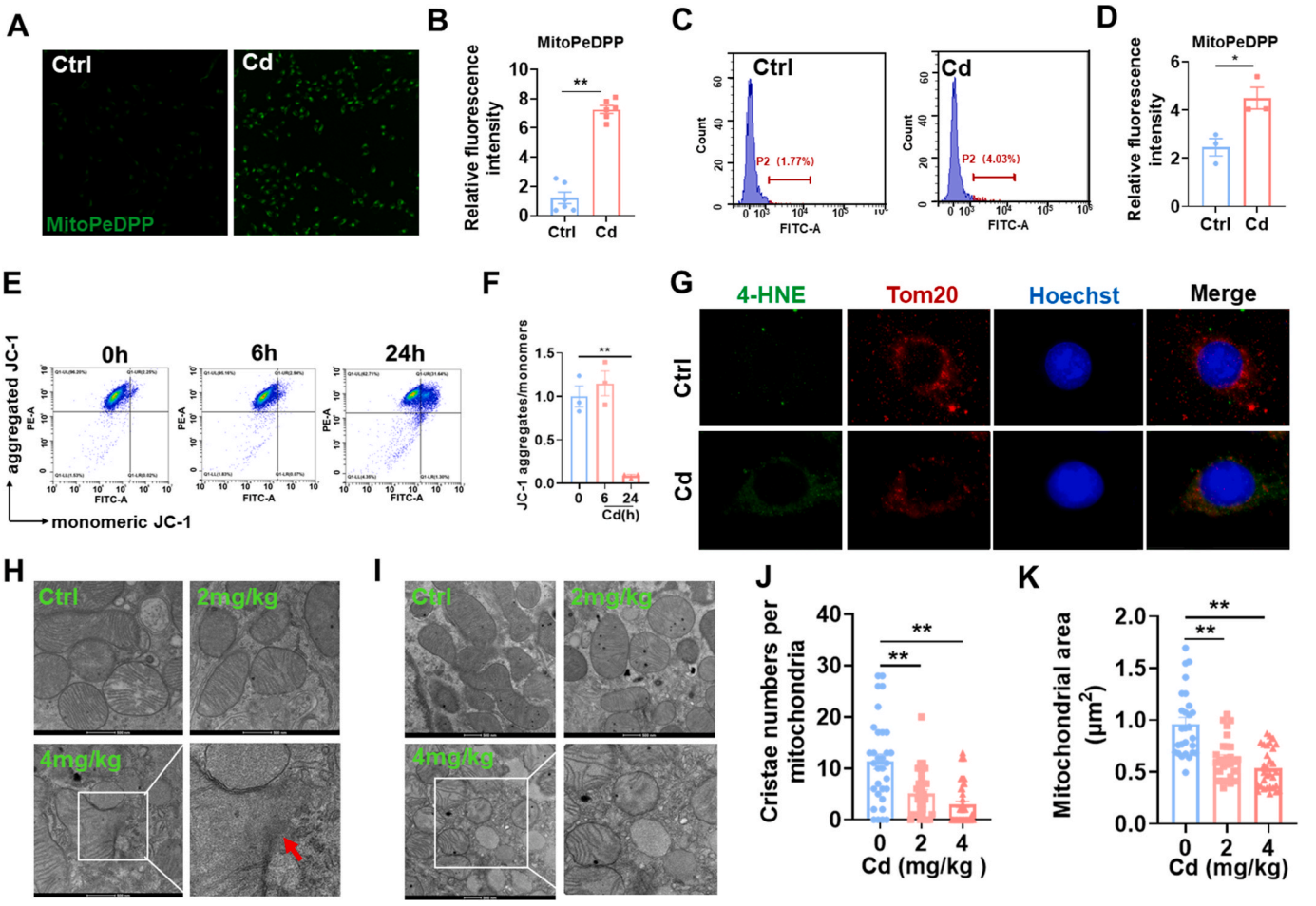

Fig. 3. Cd exposure evokes mitochondrial lipid peroxidation and mitochondrial dysfunction. HK-2 cells were co-cultivated with $CdCl_2$ (10 μM) for 24 h. (A and B) Mitochondrial oxidized lipids were determined by MitoPeDPP. (A) Representative pictures. (B) Statistical analysis. (C and D) Mitochondrial oxidized lipids were evaluated by flow cytometry. (C) Representative pictures. (D) Quantitative analysis. (E and F) MMPs were detected by JC-1 staining. (E) Representative images. (F) Statistical analysis. (G) Co-localization of 4-HNE with TOM20. (H–K) $CdCl_2$ (2 mg/kg or 4 mg/kg) was injected intraperitoneally into adult BALB/c male mice. Mitochondrial ultrastructure was evaluated by electron microscopy. (H) The integrity of mitochondrial membrane. Arrow indicates mitochondrial membrane rupture. (I–K) Mitochondrial area and cristae were analyzed. (I) Representative pictures. (J) Cristae number per mitochondrion. (K) Mitochondrial area. All data are presented as mean ± S.E.M. (N = 3). $^*P < 0.05$, $^{**}P < 0.01$.

Cd-exposed renal tubules (Fig. 3H). Finally, mitochondrial ultrastructure was further evaluated by transmission electron microscopy (Fig. 3I). The results showed that mitochondrial cristae number and area were reduced in Cd-exposed cortical renal tubules (Fig. 3J and K).

3.4. Cd induces mitochondrial SIRT3 downregulation and GPX4 acetylation

GPX4 and FSP1 are two major defensive regulators against ferroptosis [31]. Renal GPX4 and FSP1 were measured using Western blot (Fig. 4A). Renal GPX4 protein was obviously reduced (Fig. 4B), whereas no difference on renal FSP1 was shown between Cd-exposed and controls (Fig. 4C). DHODH, located in mitochondria, is another defensive regulator against ferroptosis. Renal DHODH was measured using Western blot (Fig. 4D). DHODH protein was slightly reduced in Cd-exposed mouse kidneys (Fig. 4E). Next, cytoplasmic and mitochondrial GPX4 was analyzed. Although cytoplasmic GPX4 was not changed (Fig. 4F and G), mitochondrial GPX4 was reduced in Cd-exposed mouse kidneys (Fig. 4H and I). SIRT3 is an NAD^+-dependent deacetylase that regulates mitochondrial protein stability [32]. The impact of Cd exposure on mitochondrial SIRT3 protein was evaluated (Fig. 4J). As shown in Fig. 4K, mitochondrial SIRT3 protein was reduced in Cd-exposed mouse kidneys. Mitochondrial GPX4 acetylation was analyzed by CoIP (Fig. 4L). Mitochondrial GPX4 acetylation was obviously elevated (Fig. 4M) and mitochondrial GPX4 protein was accordingly reduced (Fig. 4N) in Cd-exposed mouse kidneys. Finally, co-localization of SIRT3 with GPX4 and Mito-Tracker was observed by immunofluorescence. As shown in Fig. 4O, co-localization of SIRT3 with GPX4 and Mito-Tracker was weakened in Cd-exposed HK-2 cells.

3.5. Sirt3 knockout exacerbates Cd-induced mitochondrial GPX4 acetylation and renal cell ferroptosis

To explore the role of SIRT3 reduction on Cd-induced mitochondrial GPX4 acetylation and renal cell ferroptosis, $Sirt3^{-/-}$ mouse were constructed (Fig. 5A and B). As expected, Cd-evoked mitochondrial GPX4 acetylation was aggravated in $Sirt3^{-/-}$ mouse kidneys (Fig. 5C and D). Mitochondrial GPX4 downregulation was accordingly exacerbated in Cd-exposed $Sirt3^{-/-}$ mouse kidneys (Fig. 5C and E). Targeted metabolomics of oxidized lipids were used to determine the impact of Sirt3 knockout on Cd-induced renal cell ferroptosis (Fig. 5F). As expected, Cd-induced elevation of renal oxidized ARA metabolites was aggravated in $Sirt3^{-/-}$ mouse kidneys (Fig. 5G). Despite no impact on renal oxidized LA and ALA metabolites (Fig. 5H and I), Sirt3 knockout exacerbated Cd-induced elevation of renal oxidized EPA and DHA metabolites (Fig. 5J and K). The impact of Sirt3 knockout on Cd-evoked renal 4-HNE was

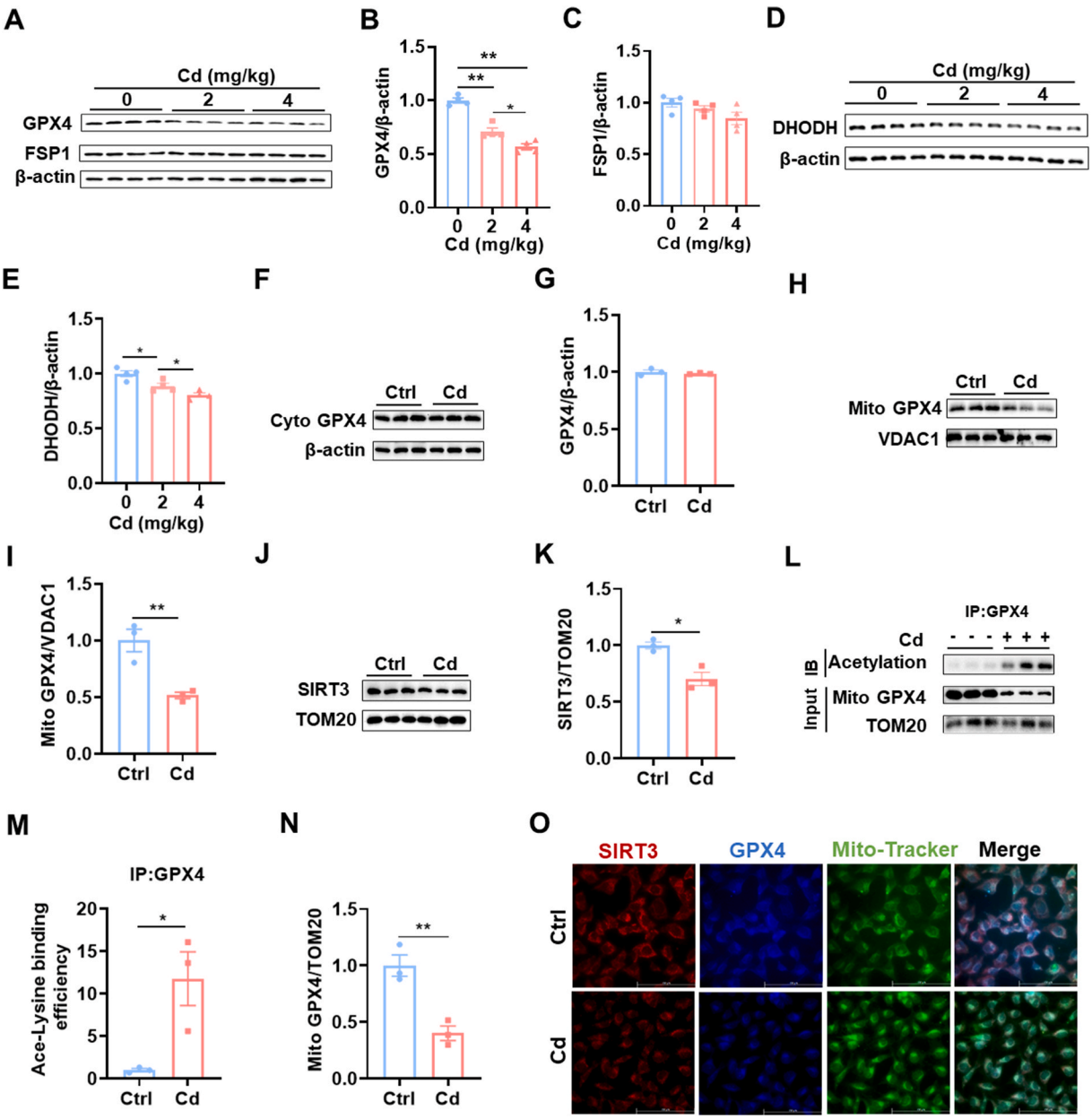

Fig. 4. Cd induces mitochondrial SIRT3 downregulation and GPX4 acetylation. $CdCl_2$ (2 mg/kg or 4 mg/kg) was injected intraperitoneally into adult BALB/c male mice. Kidney tissues were reserved 24 h after $CdCl_2$. (A–C) GPX4 and FSP1 were detected by immunoblot. (A) Representative images. (B) GPX4/β-actin; (C) FSP1/β-actin. (D–E) DHODH was detected by immunoblot. (D) Representative images. (E) DHODH/β-actin. (F–I) $CdCl_2$ (4 mg/kg) was injected intraperitoneally into adult BALB/c male mice. Kidney tissues were reserved 24 h after $CdCl_2$. Renal mitochondria and cytoplasm were extracted. (F and G) Cytoplasmic GPX4 was measured by immunoblot. (F) Representative images. (G) GPX4/β-actin. (H and I) Mitochondrial GPX4 was measured by immunoblot. (H) Representative images. (I) GPX4/VDAC1. (J and K) Mitochondrial SIRT3 was measured by immunoblot. (J) Representative images. (K) SIRT3/TOM20. (L–N) Mitochondrial GPX4 acetylation was analyzed by Co-IP. (L) Representative images. (M) Ace-Lysine binding efficiency. (N) GPX4/TOM20. (O) HK-2 cells were co-cultivated with $CdCl_2$ (10 μM) for 24 h. Co-localization of SIRT3, GPX4 and mitochondrial Tracker was observed by immunofluorescence. Red indicates SIRT3; Blue represents GPX4; Green represents Mito-Tracker. All data are presented as mean ± S.E.M. (N = 3–4). $^{*}P < 0.05$, $^{**}P < 0.01$. (For interpretation of the references to colour in this figure legend, the reader is referred to the Web version of this article.)

then evaluated. As shown in Fig. 5L and M, Cd-induced elevation of renal 4-HNE was aggravated in $Sirt3^{-/-}$ mouse. Finally, the impact of Sirt3 knockout on Cd-induced AKI was analyzed. Cd-induced pathological damage was exacerbated in $Sirt3^{-/-}$ mouse (Fig. 5N and O). In addition, Cd-induced elevation of serum UA was aggravated in $Sirt3^{-/-}$ mouse (Fig. 5P).

3.6. Pretreatment with NMN attenuates Cd-induced mitochondrial lipid peroxidation in HK-2 cells

To verify the role of SIRT3 on protecting against Cd-induced renal cell ferroptosis, the effect of pretreatment with NMN, a precursor of NAD^{+} synthesis, on Cd-induced mitochondrial lipid peroxidation was evaluated in HK-2 cells. As expected, Cd-induced mitochondrial lipid peroxidation was attenuated in NMN-pretreated HK-2 cells (Fig. 6A–D). First, the effect of NMN pretreatment on mitochondrial lipid peroxidation was detected by confocal microscopy. As shown in Fig. 6A and B,

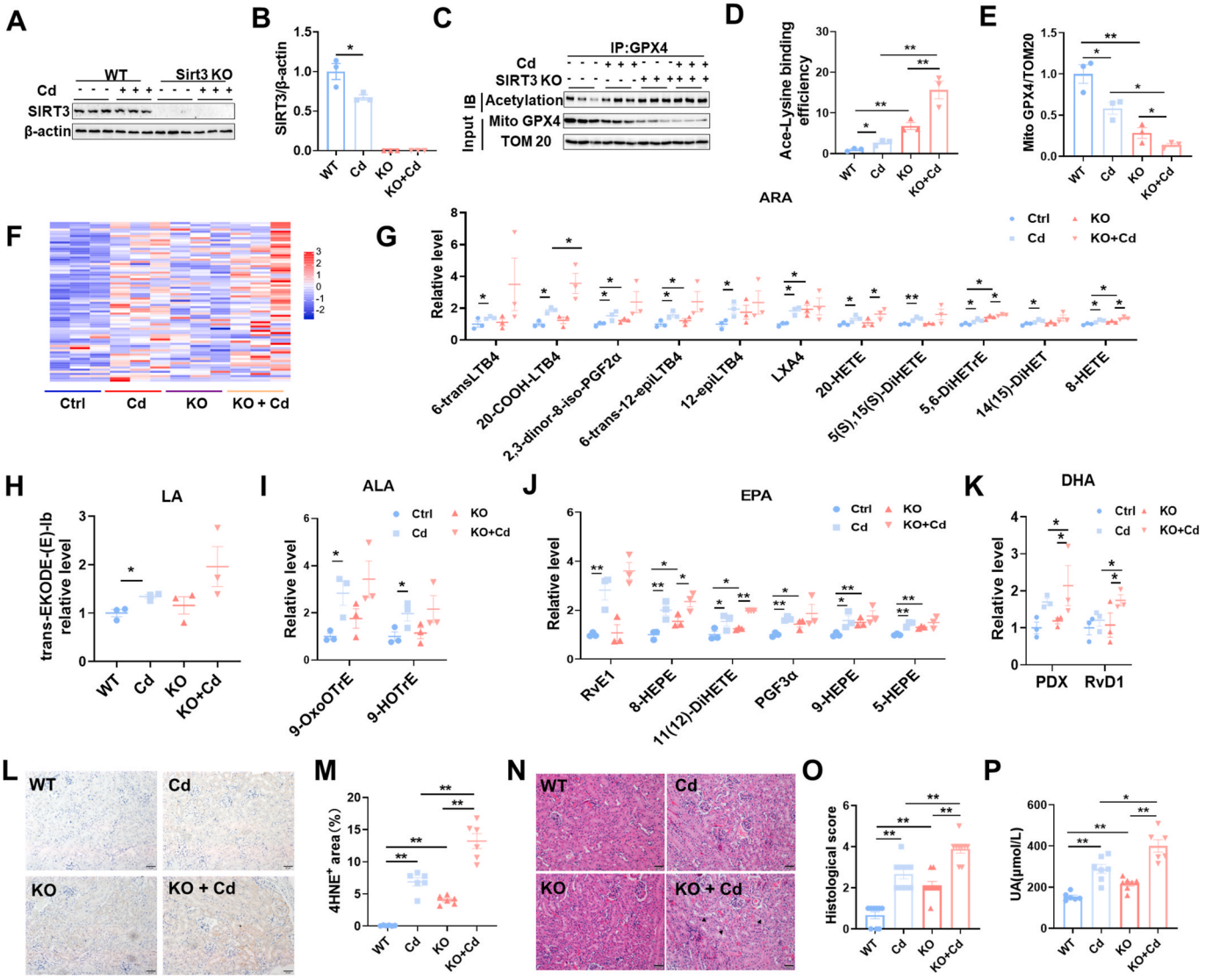

Fig. 5. Sirt3 knockout exacerbates Cd-induced mitochondrial GPX4 acetylation, renal cell ferroptosis and AKI. Wild type and *Sirt3*$^{-/-}$ male mice intraperitoneally injected with $CdCl_2$ (4 mg/kg). Kidney tissues were collected 24 h after $CdCl_2$. (A) SIRT3 was detected using immunoblot; (B) SIRT3/β-actin. (C–E) Mitochondrial GPX4 acetylation was analyzed by Co-IP. (C) Representative images. (D) Ace-Lysine binding efficiency. (E) GPX4/TOM20. (F–K) Targeted metabolomics of oxidized lipids were examined by LC-MS/MS. Renal oxidized metabolites of (F) A heatmap. (G)ARA, (H) LA, (I) ALA, (J) EPA and (K) DHA are shown. (L and M) Renal 4-HNE^{+} area was measured by IHC. (L) Representative images. (M) Quantitative analysis. (N and O) Renal pathology was evaluated. (N) Representative H&E images. (O) Pathological score. (P) Serum UA. All data are presented as mean ± S.E.M. (N = 6–8). *$P < 0.05$, **$P < 0.01$.

mitochondrial lipid peroxidation was reduced in Cd-exposed HK-2 cells after NMN with pretreatment. Mitochondrial lipid peroxidation was evaluated by flow cytometry (Fig. 6C). As shown, the mitochondrial oxidized lipid content of cadmium-exposed HK-2 was significantly increased and partially alleviated by NMN pretreatment (Fig. 6D). Next, 4-HNE and TOM20 were co-localized by immunofluorescence. Unsurprisingly, 4-HNE, which is predominantly present in mitochondria, was attenuated (Fig. 6E). In addition, oxidized lipids were evaluated using C11-BODIPY. As shown in Fig. 6F and G, oxidized lipids were attenuated in Cd-exposed HK-2 cells after NMN pretreatment. Finally, the Cd-induced reduction of MMPs was partially reversed (Fig. 6H and I).

3.7. Pretreatment with NMN attenuates Cd-induced mitochondrial GPX4 acetylation, renal cell ferroptosis and AKI

We evaluated the effect of NMN pretreatment on Cd-induced GPX4 acetylation. As expected, Cd-induced mitochondrial GPX4 acetylation was attenuated in the kidneys of NMN-pretreated mouse (Fig. 7A and B). Meanwhile, the Cd-induced reduction of mitochondrial GPX4 was correspondingly reversed in the kidneys of NMN pretreated mouse (Fig. 7A and C). Moreover, NMN pretreatment alleviated Cd-induced mitochondrial damage. Ultrastructural analysis revealed that Cd-induced mitochondrial membrane rupture was ameliorated in NMN-pretreated mouse renal tubules (Fig. 7D). Cd-induced reduction in mitochondrial cristae number and area was attenuated by NMN pretreatment (Fig. 7E–G). We evaluated the effect of NMN pretreatment on Cd-induced lipid peroxidation. Cd-induced elevation of renal MDA and 4-HNE was attenuated in NMN pretreated mouse (Fig. 7H–J). The effect of NMN pretreatment on Cd-induced oxidized lipids was detected using targeted metabolomics (Fig. 7K-P). As expected, Cd-induced oxidized ARA metabolites, a key indicator of ferroptosis, were reduced in the kidneys of NMN pretreated mouse (Fig. 7L). In addition, Cd-induced oxidized metabolites, including LA, ALA, EPA, and DHA, were also attenuated in the kidneys of NMN pretreated mouse (Fig. 7M – P). Finally, the effect of NMN pretreatment on Cd-induced AKI was assessed. As shown in Fig. 7Q and R, NMN pretreated mouse kidneys

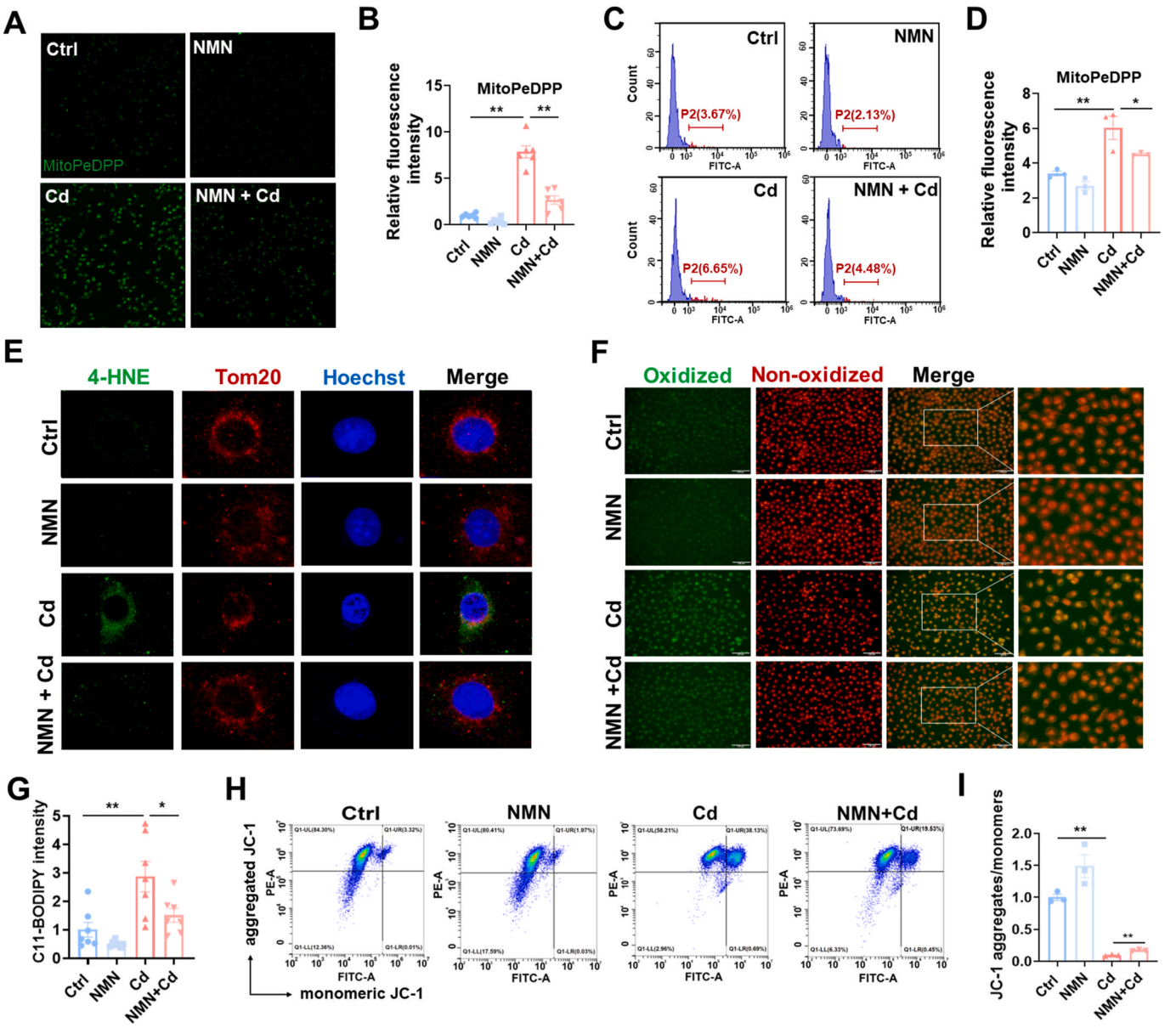

Fig. 6. Pretreatment with NMN attenuates Cd-induced mitochondrial lipid peroxidation in HK-2 cells. HK-2 cells were co-cultivated with $CdCl_2$ (10 μM) for 24 h. Some HK-2 cells were pretreated with NMN (1 mM) for 2 h before Cd exposure. (A and B) Mitochondrial oxidized lipids were measured using confocal microscopy. (A) Representative pictures. (B) Statistical analysis. (C and D) Mitochondrial oxidized lipids were evaluated using flow cytometry. (C) Representative pictures. (D) Statistical analysis. (E) Co-localization of 4-HNE with TOM20 was evaluated using immunofluorescence. (F and G) Oxidized lipids were measured by C11-BODIPY staining. (F) Representative pictures. (G) Statistical analysis. (H and I) MMPs were detected using JC-1 staining. (H) Representative pictures. (I) Statistical analysis. All data are presented as mean ± S.E.M. (N = 3). $^{*}P < 0.05$, $^{**}P < 0.01$.

ameliorated Cd-induced pathological injury. In addition, Cd-induced elevation of serum UA was attenuated in NMN pretreated mouse (Fig. 7S).

4. Discussion

In this study, we aimed to investigate the impacts of acute Cd exposure on renal cell ferroptosis. The novel findings are as follow: (1) mitochondrial oxidized lipids were elevated in Cd-exposed mouse kidneys and HK-2 cells; (2) mitochondrial SIRT3 was downregulated and mitochondrial GPX4 acetylation was elevated; (3) Cd-induced mitochondrial GPX4 acetylation and renal cell ferroptosis were exacerbated in Sirt3$^{-/-}$ mouse kidneys; (4) Cd-induced mitochondrial GPX4 acetylation and renal cell ferroptosis were attenuated in NMN-pretreated HK-2 cells and mouse kidneys. These results suggest that mitochondrial GPX4 acetylation, probably caused by SIRT3 reduction, is involved in Cd-induced renal cell ferroptosis.

It is well known that long-term Cd exposure, even at a low concentration, causes renal Cd accumulation [33]. Numerous epidemiological data have demonstrated that long-term Cd exposure is associated with the increased risk of chronic kidney disease [34]. On the other hand, animal experiments indicated that acute Cd exposure caused nephrotoxicity [35]. Two recent studies showed that subacute exposure to $CdCl_2$ (2 mg/kg/day) for one week or two weeks caused elevation of BUN and destruction of renal tubular structure [36,37]. In this study, mice were injected with a single dose of $CdCl_2$ (2 or 4 mg/kg) and found that exposure to a higher dose of $CdCl_2$ (4 mg/kg) for 24 h induced AKI, as determined by renal pathology, serum UA, and elevated expression of Kim-1 in mouse kidneys. Renal pathology showed nuclear consolidation and brush border detachment in Cd-exposed mouse kidneys.

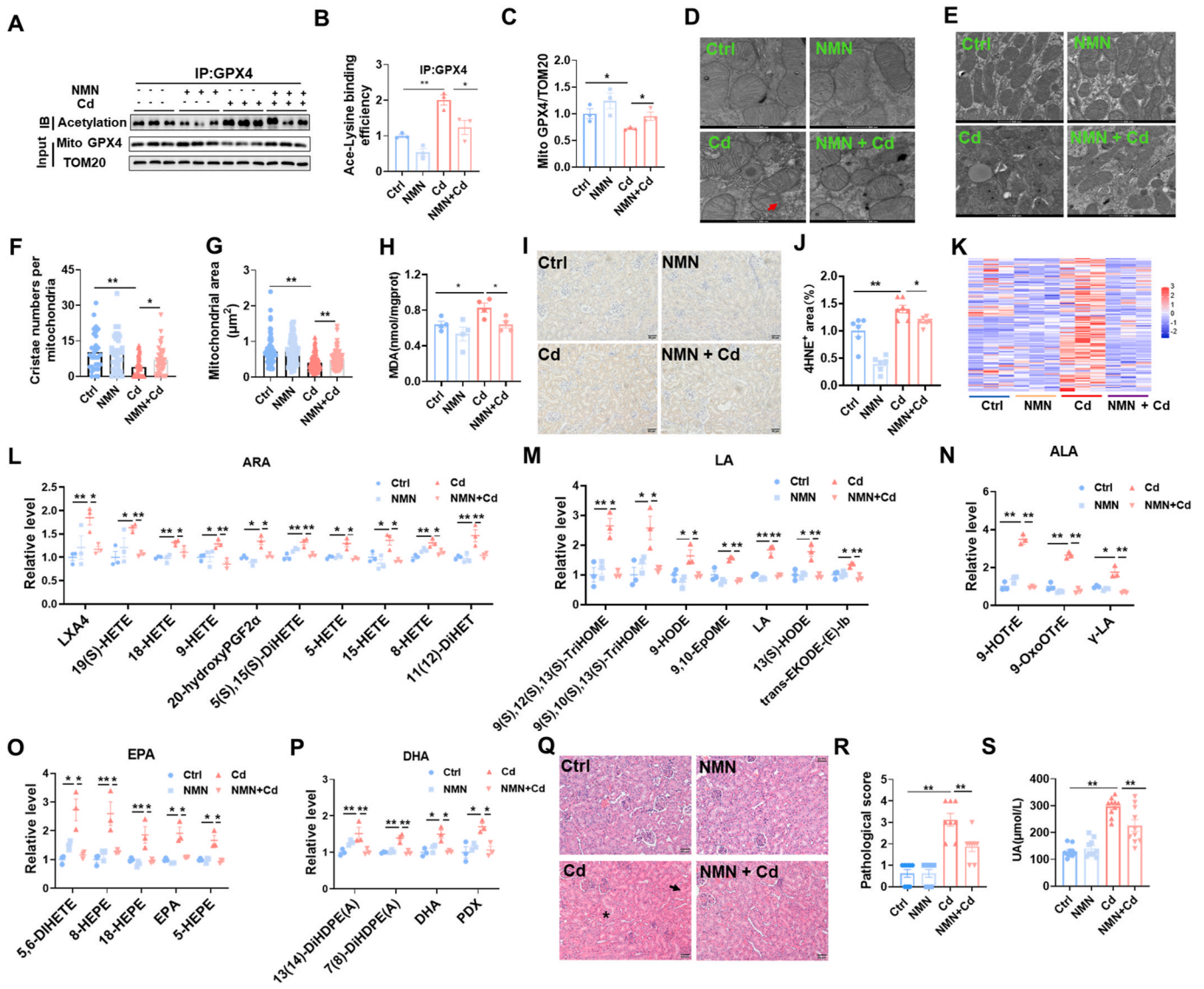

Fig. 7. Pretreatment with NMN attenuates Cd-induced mitochondrial GPX4 acetylation, renal cell ferroptosis and AKI. All mice except controls were intraperitoneally injected with $CdCl_2$ (4 mg/kg). Some mice were pretreated with NMN (500 mg/kg) for 5 consecutive days. Kidney tissues were reserved 24 h after $CdCl_2$. (A–C) Renal mitochondria was extracted. Mitochondrial GPX4 acetylation was analyzed by Co-IP. (A) Representative images. (B) Ace-Lysine binding efficiency. (C) GPX4/TOM20. (D–G) Mitochondrial ultrastructure was evaluated by electron microscopy. (D) The integrity of mitochondrial membrane. Arrow indicates mitochondrial membrane rupture. (E–G) Mitochondrial area and cristae were analyzed. (E) Representative images. (F) Cristae number per mitochondrion. (G) Mitochondrial area. (H)Renal MDA content. (I and J) Renal 4-HNE^+ area was measured by IHC. (I) Representative images. (J) Quantitative analysis. (K–P) Targeted metabolomics of oxidized lipids were examined by LC-MS/MS. Renal oxidized metabolites of (K) A heatmap. (L) ARA, (M) LA, (N) ALA, (O) EPA and (P) DHA were shown. (Q and R) Renal pathology was evaluated. (Q) Representative H&E images. (R) Pathological scores. (S) Serum UA. All data are presented as mean ± S.E.M. (N = 6–8). $^*P < 0.05$, $^{**}P < 0.01$.

Time-course analysis found that pathological damage began at 12 h and aggravated at 24 h after mice were exposed to $CdCl_2$ (4 mg/kg). In addition, serum UA was elevated, beginning 12 h and further aggravating 24 h after mice were exposed to $CdCl_2$ (4 mg/kg). These results suggest that exposure to a high dose of Cd, even a single dose, could induce AKI.

In the past, numerous studies focused on renal cell apoptosis during Cd-induced AKI [38,39]. A recent study indicated that acute Cd exposure caused renal cell necroptosis [37]. Ferroptosis is a novel regulatory cell death, characterized by intracellular free iron overload and membrane lipid peroxidation [40]. Recently, an animal experiment found that renal MDA and ferrous contents were elevated in Cd-exposed mice [19]. The in vitro experiment showed that ferrinstain-1 (Fer-1), a ferroptotic inhibitor, alleviated Cd-induced cell death [19]. In this study, we showed that ferroptotic pathway, as determined by RNA sequencing and transcriptomics analyses, was enriched in Cd-exposed mouse kidneys. Renal MDA content and 4-HNE^+ area, two ferroptotic indicators, were elevated in Cd-exposed mouse. It is widely believed that oxidized ARA metabolites are the major oxidized lipids in ferroptosis [41]. In the current study, targeted metabolomics was used to analyze renal oxidized lipid metabolites. The results showed that all oxidized ARA metabolites were increased in Cd-exposed mouse kidneys. Renal oxidized metabolites of other unsaturated fatty acids, including EPA, DHA, ALA, and LA, were upregulated in Cd-exposed mice. Moreover, mitochondrial oxidized lipids, determined by IF and flow cytometry, were obviously elevated in Cd-exposed HK-2 cells. Immunofluorescence co-localization confirmed that Cd-evoked oxidized lipids were mainly distributed in mitochondria. Mitochondrial ultrastructure showed a mitochondrial membrane rupture in Cd-exposed mouse kidneys. Renal mitochondrial cristae were accordingly reduced in Cd-exposed mouse. Our results

provide novel evidences that acute Cd exposure causes renal cell ferroptosis.

GPX4 and FSP1 are two well-known defensive regulators against ferroptosis [42]. In this study, our results showed that acute Cd exposure had little impact on renal FSP1 expression. Interestingly, GPX4 protein was obviously downregulated in Cd-exposed mouse kidneys. It is widely believed that GPX4 is distributed in both mitochondria and cytoplasm [43]. In this study, we found that mitochondrial GPX4 level was reduced, whereas cytoplasmic GPX4 was not changed in Cd-exposed mouse kidneys. SIRT3, an NAD^+-dependent deacetylase, participates in the regulation of mitochondrial protein stability by inhibiting mitochondrial protein acetylation [32]. Several studies have confirmed that mitochondrial SIRT3 downregulation is involved in cisplatin and ischemia-reperfusion-induced AKI [44,45]. The current study found that mitochondrial SIRT3 was reduced in Cd-exposed mouse kidneys and HK-2 cells. Conversely, mitochondrial GPX4 acetylation was elevated in Cd-exposed mouse kidneys. To explore whether SIRT3 reduction is involved in Cd-evoked mitochondrial GPX4 acetylation and subsequent renal cell ferroptosis, mitochondrial GPX4 acetylation was detected in $Sirt3^{-/-}$ mouse kidneys. As expected, renal mitochondrial GPX4 acetylation was increased in *Sirt3*$^{-/-}$ mouse. Moreover, Cd-evoked mitochondrial GPX4 acetylation was aggravated in *Sirt3*$^{-/-}$ mouse kidneys. Importantly, Cd-induced oxidized lipids and AKI were exacerbated in *Sirt3*$^{-/-}$ mouse kidneys. NMN is a precursor of NAD^+ synthesis [46]. Accumulating data have demonstrated that NMN could activate mitochondrial SIRT3 signaling [47,48]. To further confirm whether mitochondrial SIRT3 reduction is involved in Cd-induced renal cell ferroptosis, the effect of pretreatment with NMN on mitochondrial lipid peroxidation was analyzed in Cd-exposed HK-2 cells and mouse kidneys. The in vitro experiments showed that pretreatment with NMN alleviated mitochondrial function and attenuated oxidized lipids in Cd-exposed HK-2 cells. The in vivo experiments found that pretreatment with NMN attenuated mitochondrial GPX4 acetylation in Cd-exposed mouse kidneys. In addition, NMN pretreatment alleviated mitochondrial dysfunction and renal lipid peroxidation in Cd-exposed mouse. Importantly, NMN pretreatment protected against Cd-induced AKI. Taken together, these results suggest that mitochondrial GPX4 acetylation, probably caused by SIRT3 reduction, partially contribute to Cd-induced renal cell ferroptosis.

Our findings have significant translational implications. An early report showed that supplementation with NMN prevented mitochondrial dysfunction in a rat model of hemorrhagic shock [49]. Recently, two studies demonstrated that supplementation with NMN prevented endotoxin and ischemia/reperfusion induced AKI through improving mitochondrial function [29,50]. In this study, we found that pretreatment with NMN attenuated Cd-induced renal cell ferroptosis by inhibiting mitochondrial GPX4 acetylation. These findings provide new evidence that NAD^+ precursor could be used to prevent environmental stress-induced AKI. The current results confirmed that mitochondrial GPX4 acetylation, probably caused by SIRT3 downregulation, is partially involved in Cd-induced renal cell ferroptosis. However, the current study has several limitations. Firstly, the current study did not investigate the role of other SIRT deacetylases, such as mitochondrial SIRT4 and SIRT5, on Cd-evoked mitochondrial GPX4 acetylation. Secondly, the current study did not explore the role of mitochondrial acetylases, such as GCN5L, on Cd-evoked mitochondrial GPX4 acetylation. Several studies found that atorvastatin, an inhibitor of cholesterol synthesis, inhibited isoproterenol (ISO)-induced ferroptosis [51]. Thus, additional work is required to explore the protective effect of treatment with statin on Cd-induced ferroptosis and AKI.

In summary, the current study investigated the impact of acute Cd exposure on renal cell ferroptosis. We showed that acute Cd exposure caused mitochondrial lipid peroxidation in mouse kidneys and HK-2 cells. Mechanistically, acute Cd exposure induced mitochondrial SIRT3 downregulation and GPX4 acetylation. Sirt3 knockout exacerbated Cd-induced mitochondrial GPX4 acetylation and renal cell ferroptosis. Conversely, pretreatment with NMN attenuated Cd-induced GPX4 acetylation and renal cell ferroptosis. Our results provide experimental evidences that mitochondrial GPX4 acetylation, probably caused by SIRT3 downregulation, is partially involved in Cd-induced renal cell ferroptosis (Fig. 8). NMN, an NAD^+ precursor, could be used to prevent environmental stress induced AKI by restoring mitochondrial SIRT3 activity.

Funding

This work was supported by National Natural Science Foundation of China (82204493), Anhui Provincial Natural Science Foundation of China (2208085QH237), and Promotion project of basic and clinical collaborative research from Anhui Medical University of China (2020xkjT038).

CRediT authorship contribution statement

Yue-Yue Guo: Conceptualization, Writing – original draft, Writing – review & editing. **Nan-Nan Liang:** Conceptualization, Writing – original draft. **Xiao-Yi Zhang:** Conceptualization, Writing – original draft. **Ya-Hui Ren:** Resources. **Wen-Zheng Wu:** Resources. **Zhi-Bing Liu:** Resources. **Yi-Zhang He:** Resources. **Yi-Hao Zhang:** Methodology. **Yi-Chao Huang:** Investigation. **Tao Zhang:** Investigation. **De-Xiang Xu:** Conceptualization, Supervision, Writing – review & editing. **Shen Xu:** Funding acquisition, Supervision, Writing – review & editing, Conceptualization.

Declaration of competing interest

The authors declare that they have no known competing financial interests or personal relationships that could have appeared to influence

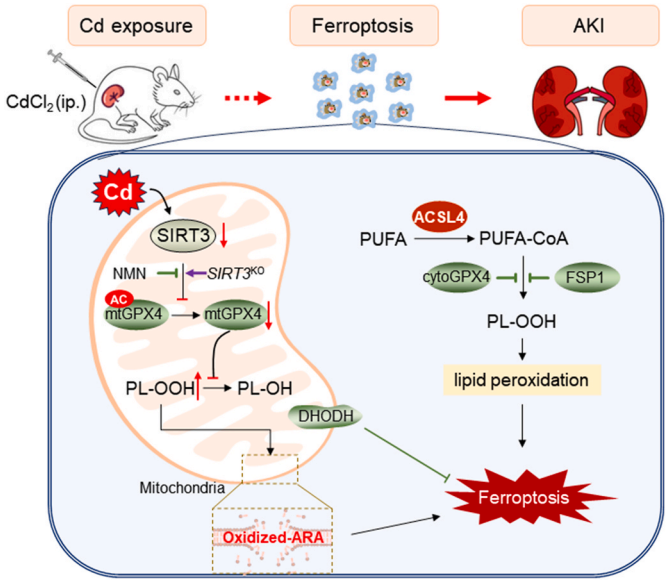

Fig. 8. Role of mitochondrial GPX4 acetylation in Cd-induced renal cell ferroptosis and acute kidney injury. Briefly, acute Cd exposure reduces mitochondrial SIRT3, resulting in mitochondrial GPX4 acetylation and mitochondrial GPX4 reduction in mouse kidney. Mitochondrial GPX4 reduction induces elevation of mitochondrial oxidized lipids, mainly oxidized ARA, subsequently renal cell ferroptosis and acute kidney injury. Mitochondrial GPX4 acetylation, probably caused by SIRT3 reduction, is partially involved in Cd-induced renal cell ferroptosis. ACSL4: Acyl-CoA synthetase long chain family member 4; AKI: Acute kidney injury; ARA: arachidonic acid; $CdCl_2$: Cadmium dichloride; DHODH: Dihydroorotate dehydrogenase; FSP1: Ferroptosis suppressor protein 1; GPX4: Glutathione peroxidase 4; NMN: Beta-Nicotinamide Mononucleotide; PUFA: Polyunsaturated fatty acids; SIRT3: Sirtuin 3.

the work reported in this paper.

Appendix A. Supplementary data

Supplementary data to this article can be found online at https://doi.org/10.1016/j.redox.2024.103179.

References

[1] P. Pickkers, M. Darmon, E. Hoste, M. Joannidis, M. Legrand, M. Ostermann, J. R. Prowle, A. Schneider, M. Schetz, Acute kidney injury in the critically ill: an updated review on pathophysiology and management, Intensive Care Med. 47 (8) (2021) 835–850.

[2] H. Scholz, F.J. Boivin, K.M. Schmidt-Ott, S. Bachmann, K.U. Eckardt, U.I. Scholl, P. B. Persson, Kidney physiology and susceptibility to acute kidney injury: implications for renoprotection, Nat. Rev. Nephrol. 17 (5) (2021) 335–349.

[3] S. Peerapornratana, C.L. Manrique-Caballero, H. Gómez, J.A. Kellum, Acute kidney injury from sepsis: current concepts, epidemiology, pathophysiology, prevention and treatment, Kidney Int. 96 (5) (2019) 1083–1099.

[4] M.A. Perazella, M.H. Rosner, Drug-induced acute kidney injury, Clin. J. Am. Soc. Nephrol.: CJASN 17 (8) (2022) 1220–1233.

[5] J. Min, D.H. Kang, C. Kang, M.L. Bell, H. Kim, J. Yang, A. Gasparrini, E. Lavigne, M. Hashizume, Y. Kim, C. Fook Sheng Ng, Y. Honda, S. das Neves Pereira da Silva, J. Madureira, Y. Leon Guo, S.C. Pan, B. Armstrong, F. Sera, P. Masselot, J. Schwartz, W. Lee, Fluctuating risk of acute kidney injury-related mortality for four weeks after exposure to air pollution: a multi-country time-series study in 6 countries, Environ. Int. 183 (2024) 108367.

[6] W. Lee, X. Wu, S. Heo, J.M. Kim, K.C. Fong, J.Y. Son, M.B. Sabath, A. Trisovic, D. Braun, J.Y. Park, Y.C. Kim, J.P. Lee, J. Schwartz, H. Kim, F. Dominici, Z. Al-Aly, M.L. Bell, Air pollution and acute kidney injury in the U.S. Medicare population: a longitudinal cohort study, Environ. Health Perspect. 131 (4) (2023) 47008.

[7] P.G. Peera Sheikh Kulsum, R. Khanam, S. Das, A.K. Nayak, F.M.G. Tack, E. Meers, M. Vithanage, M. Shahid, A. Kumar, S. Chakraborty, T. Bhattacharya, J.K. Biswas, A state-of-the-art review on cadmium uptake, toxicity, and tolerance in rice: from physiological response to remediation process, Environ. Res. 220 (2023) 115098.

[8] M. Wacewicz-Muczyńska, K. Socha, J. Soroczyńska, M. Niczyporuk, M. H. Borawska, Cadmium, lead and mercury in the blood of psoriatic and vitiligo patients and their possible associations with dietary habits, Sci. Total Environ. 757 (2021) 143967.

[9] Z. Yuan, T. Luo, X. Liu, H. Hua, Y. Zhuang, X. Zhang, L. Zhang, Y. Zhang, W. Xu, J. Ren, Tracing anthropogenic cadmium emissions: from sources to pollution, Sci. Total Environ. 676 (2019) 87–96.

[10] M. Zou, S. Zhou, Y. Zhou, Z. Jia, T. Guo, J. Wang, Cadmium pollution of soil-rice ecosystems in rice cultivation dominated regions in China: a review, Environ. Pollut. 280 (2021) 116965.

[11] S.U. Rahman, J.C. Han, M. Ahmad, S. Gao, K.A. Khan, B. Li, Y. Zhou, X. Zhao, Y. Huang, Toxic effects of lead (Pb), cadmium (Cd) and tetracycline (TC) on the growth and development of Triticum aestivum: a meta-analysis, Sci. Total Environ. 904 (2023) 166677.

[12] Y.L. Ji, H. Wang, X.F. Zhao, Q. Wang, C. Zhang, Y. Zhang, M. Zhao, Y.H. Chen, X. H. Meng, D.X. Xu, Crosstalk between endoplasmic reticulum stress and mitochondrial pathway mediates cadmium-induced germ cell apoptosis in testes, Toxicol. Sci.: an official journal of the Society of Toxicology 124 (2) (2011) 446–459.

[13] R. Pouillot, S. Santillana Farakos, J.M. Van Doren, Modeling the risk of low bone mass and osteoporosis as a function of urinary cadmium in U.S adults aged 50-79 years, Environ. Res. 212 (Pt B) (2022) 113315.

[14] W.J. Wang, K. Peng, X. Lu, Y.Y. Zhu, Z. Li, Q.H. Qian, Y.X. Yao, L. Fu, Y. Wang, Y. C. Huang, H. Zhao, H. Wang, D.X. Xu, Z.X. Tan, Long-term cadmium exposure induces chronic obstructive pulmonary disease-like lung lesions in a mouse model, Sci. Total Environ. 879 (2023) 163073.

[15] Y. Zhang, X. Gong, R. Li, W. Gao, D. Hu, X. Yi, Y. Liu, J. Fang, J. Shao, Y. Ma, L. Jin, Exposure to cadmium and lead is associated with diabetic kidney disease in diabetic patients, Environ. Health: a global access science source 23 (1) (2024) 1.

[16] J. Zhang, Y. Wang, L. Fu, B. Wang, Y.L. Ji, H. Wang, D.X. Xu, Chronic cadmium exposure induced hepatic cellular stress and inflammation in aged female mice, J. Appl. Toxicol.: JAT. 39 (3) (2019) 498–509.

[17] X. Chen, X. Chen, Y. Wang, X. Wang, M. Wang, Y. Liang, G. Zhu, T. Jin, A nomogram for predicting the renal dysfunction in a Chinese population with reduction in cadmium exposure based on an 8 years follow up study, Ecotoxicol. Environ. Saf. 191 (2020) 110251.

[18] X. Feng, X. Jin, R. Zhou, Q. Jiang, Y. Wang, X. Zhang, K. Shang, J. Zhang, C. Yu, J. Shou, Deep learning approach identified a gene signature predictive of the severity of renal damage caused by chronic cadmium accumulation, J. Hazard Mater. 433 (2022) 128795.

[19] Z.G. Gong, Y. Zhao, Z.Y. Wang, R.F. Fan, Z.P. Liu, L. Wang, Epigenetic regulator BRD4 is involved in cadmium-induced acute kidney injury via contributing to lysosomal dysfunction, autophagy blockade and oxidative stress, J. Hazard Mater. 423 (Pt A) (2022) 127110.

[20] C. Zhao, D. Yu, Z. He, L. Bao, L. Feng, L. Chen, Z. Liu, X. Hu, N. Zhang, T. Wang, Y. Fu, Endoplasmic reticulum stress-mediated autophagy activation is involved in cadmium-induced ferroptosis of renal tubular epithelial cells, Free Radic. Biol. Med. 175 (2021) 236–248.

[21] A.B. Sanz, M.D. Sanchez-Niño, A.M. Ramos, A. Ortiz, Regulated cell death pathways in kidney disease, Nature reviews, Nephrology 19 (5) (2023) 281–299.

[22] C. Tang, M.J. Livingston, Z. Liu, Z. Dong, Autophagy in kidney homeostasis and disease, Nat. Rev. Nephrol. 16 (9) (2020) 489–508.

[23] A. Pefanis, F.L. Ierino, J.M. Murphy, P.J. Cowan, Regulated necrosis in kidney ischemia-reperfusion injury, Kidney Int. 96 (2) (2019) 291–301.

[24] D. Liang, A.M. Minikes, X. Jiang, Ferroptosis at the intersection of lipid metabolism and cellular signaling, Mol. Cell 82 (12) (2022) 2215–2227.

[25] J.P. Friedmann Angeli, M. Schneider, B. Proneth, Y.Y. Tyurina, V.A. Tyurin, V. J. Hammond, N. Herbach, M. Aichler, A. Walch, E. Eggenhofer, D. Basavarajappa, O. Rådmark, S. Kobayashi, T. Seibt, H. Beck, F. Neff, I. Esposito, R. Wanke, H. Förster, O. Yefremova, M. Conrad, Inactivation of the ferroptosis regulator Gpx4 triggers acute renal failure in mice, Nat. Cell Biol. 16 (12) (2014) 1180–1191.

[26] J. Liu, R. Kang, D. Tang, Signaling pathways and defense mechanisms of ferroptosis, FEBS J. 289 (22) (2022) 7038–7050.

[27] E. Mishima, J. Ito, Z. Wu, T. Nakamura, A. Wahida, S. Doll, W. Tonnus, P. Nepachalovich, E. Eggenhofer, M. Aldrovandi, B. Henkelmann, K.I. Yamada, J. Wanninger, O. Zilka, E. Sato, R. Feederle, D. Hass, A. Maida, A.S.D. Mourão, A. Linkermann, M. Conrad, A non-canonical vitamin K cycle is a potent ferroptosis suppressor, Nature 608 (7924) (2022) 778–783.

[28] Y. Guan, S.R. Wang, X.Z. Huang, Q.H. Xie, Y.Y. Xu, D. Shang, C.M. Hao, Nicotinamide mononucleotide, an NAD+ precursor, rescues age-associated susceptibility to AKI in a sirtuin 1-dependent manner, J. Am. Soc. Nephrol. 28 (8) (2017) 2337–2352.

[29] R. Duan, Y. Li, R. Zhang, X. Hu, Y. Wang, J. Zeng, M. Gao, Reversing acute kidney injury through coordinated interplay of anti-inflammation and iron supplementation, Adv. Mater. 35 (28) (2023) e2301283.

[30] Y. Chang, Z. Han, Y. Zhang, Y. Zhou, Z. Feng, L. Chen, X. Li, L. Li, J.Q. Si, G protein-coupled estrogen receptor activation improves contractile and diastolic functions in rat renal interlobular artery to protect against renal ischemia reperfusion injury, Biomed. Pharmacother. 112 (2019) 108666.

[31] H. Wang, C. Liu, Y. Zhao, G. Gao, Mitochondria regulation in ferroptosis, Eur. J. Cell Biol. 99 (1) (2020) 151058.

[32] M. Liu, X.Y. Kong, Y. Yao, X.A. Wang, W. Yang, H. Wu, S. Li, J.W. Ding, J. Yang, The critical role and molecular mechanisms of ferroptosis in antioxidant systems: a narrative review, Ann. Transl. Med. 10 (6) (2022) 368.

[33] J. Zhang, H. Xiang, J. Liu, Y. Chen, R.R. He, B. Liu, Mitochondrial Sirtuin 3: new emerging biological function and therapeutic target, Theranostics 10 (18) (2020) 8315–8342.

[34] C. Doccioli, F. Sera, A. Francavilla, A. Cupisti, A. Biggeri, Association of cadmium environmental exposure with chronic kidney disease: a systematic review and meta-analysis, Sci. Total Environ. 906 (2024) 167165.

[35] C.J. Bautista, N. Arango, C. Plata, I.B. Mitre-Aguilar, J. Trujillo, V. Ramírez, Mechanism of cadmium-induced nephrotoxicity, Toxicology 502 (2024) 153726.

[36] C. Chen, X. Han, G. Wang, D. Liu, L. Bao, C. Jiao, J. Luan, Y. Hou, Y. Xu, H. Wang, Q. Zhang, H. Zhou, J. Fu, J. Pi, Nrf2 deficiency aggravates the kidney injury induced by subacute cadmium exposure in mice, Arch. Toxicol. 95 (3) (2021) 883–893.

[37] X. Zheng, F. Deng, I. Sharma, Y.S. Kanwar, Myo-inositol oxygenase overexpression exacerbates cadmium-induced kidney injury via oxidant stress and necroptosis, Am. J. Physiol. Ren. Physiol. 322 (3) (2022) F344–F359.

[38] X. Chou, K. Ma, Y. Shen, Z. Min, Q. Wu, D. Sun, Dual role of inositol-requiring enzyme 1α (IRE-1α) in Cd-induced apoptosis in human renal tubular epithelial cells: endoplasmic reticulum stress and STAT3 signaling activation, Toxicology 456 (2021) 152769.

[39] A.R. Nair, W.K. Lee, K. Smeets, Q. Swennen, A. Sanchez, F. Thévenod, A. Cuypers, Glutathione and mitochondria determine acute defense responses and adaptive processes in cadmium-induced oxidative stress and toxicity of the kidney, Arch. Toxicol. 89 (12) (2015) 2273–2289.

[40] B. Wang, Y. Wang, J. Zhang, C. Hu, J. Jiang, Y. Li, Z. Peng, ROS-induced lipid peroxidation modulates cell death outcome: mechanisms behind apoptosis, autophagy, and ferroptosis, Arch. Toxicol. 97 (6) (2023) 1439–1451.

[41] Q.Z. Tuo, Y. Liu, Z. Xiang, H.F. Yan, T. Zou, Y. Shu, X.L. Ding, J.J. Zou, S. Xu, F. Tang, Y.Q. Gong, X.L. Li, Y.J. Guo, Z.Y. Zheng, A.P. Deng, Z.Z. Yang, W.J. Li, S. T. Zhang, S. Ayton, A.I. Bush, P. Lei, Thrombin induces ACSL4-dependent ferroptosis during cerebral ischemia/reperfusion, Signal Transduct. Targeted Ther. 7 (1) (2022) 59.

[42] Y. Lv, M. Wu, Z. Wang, J. Wang, Ferroptosis: from regulation of lipid peroxidation to the treatment of diseases, Cell Biol. Toxicol. 39 (3) (2023) 827–851.

[43] B. Speckmann, H.J. Bidmon, A. Pinto, M. Anlauf, H. Sies, H. Steinbrenner, Induction of glutathione peroxidase 4 expression during enterocytic cell differentiation, J. Biol. Chem. 286 (12) (2011) 10764–10772.

[44] L. Perico, M. Morigi, C. Rota, M. Breno, C. Mele, M. Noris, M. Introna, C. Capelli, L. Longaretti, D. Rottoli, S. Conti, D. Corna, G. Remuzzi, A. Benigni, Human mesenchymal stromal cells transplanted into mice stimulate renal tubular cells and enhance mitochondrial function, Nat. Commun. 8 (1) (2017) 983.

[45] L. Shen, Q. Zhang, S. Tu, W. Qin, SIRT3 mediates mitofusin 2 ubiquitination and degradation to suppress ischemia reperfusion-induced acute kidney injury, Exp. Cell Res. 408 (2) (2021) 112861.

[46] Q. Song, X. Zhou, K. Xu, S. Liu, X. Zhu, J. Yang, The safety and antiaging effects of nicotinamide mononucleotide in human clinical trials: an update, Adv. Nutr. 14 (6) (2023) 1416–1435.

[47] L.W. Liu, Y. Xie, G.Q. Li, T. Zhang, Y.H. Sui, Z.J. Zhao, Y.Y. Zhang, W.B. Yang, X. L. Geng, D.B. Xue, H. Chen, Y.W. Wang, T.Q. Lu, L.R. Shang, Z.B. Li, L. Li, B. Sun, Gut microbiota-derived nicotinamide mononucleotide alleviates acute pancreatitis

by activating pancreatic SIRT3 signalling, Br. J. Pharmacol. 180 (5) (2023) 647–666.
[48] Y. Song, S. Li, W. Geng, R. Luo, W. Liu, J. Tu, K. Wang, L. Kang, H. Yin, X. Wu, Y. Gao, Y. Zhang, C. Yang, Sirtuin 3-dependent mitochondrial redox homeostasis protects against AGEs-induced intervertebral disc degeneration, Redox Biol. 19 (2018) 339–353.
[49] C.A. Sims, Y. Guan, S. Mukherjee, K. Singh, P. Botolin, A. Davila Jr., J.A. Baur, Nicotinamide mononucleotide preserves mitochondrial function and increases survival in hemorrhagic shock, JCI insight 3 (17) (2018) e120182.
[50] S. He, Q. Gao, X. Wu, J. Shi, Y. Zhang, J. Yang, X. Li, S. Du, Y. Zhang, J. Yu, NAD^+ ameliorates endotoxin-induced acute kidney injury in a sirtuin1-dependent manner via GSK-3β/Nrf2 signalling pathway, J. Cell Mol. Med. 26 (7) (2022) 1979–1993.
[51] D. Ning, X. Yang, T. Wang, Q. Jiang, J. Yu, D. Wang, Atorvastatin treatment ameliorates cardiac function and remodeling induced by isoproterenol attack through mitigation of ferroptosis, Biochem. Biophys. Res. Commun. 574 (2021) 39–47.